Synthesis and Characteristics of Poly[*N*,*N*′-diphenyl-*N*,*N*′-bis(4-aminobiphenyl)-(1,1′-biphenyl)-4,4′-diamine pyromellitimide] as a Hole Injecting and Transporting Layer for Hybrid Organic Light-Emitting Device

Youngkyoo Kim* and Kijong Han

New Electroluminescent Systems Center, Institute for Advanced Engineering (IAE), Yongin P.O. Box 25, Kyounggi-Do 449-860, Korea

Chang-Sik Ha

Department of Polymer Science and Engineering, Pusan National University, Pusan 609-735, Korea

Received May 6, 2002; Revised Manuscript Received August 6, 2002

ABSTRACT: A novel hole injecting and transporting polymer, poly[*N*,*N*′-diphenyl-*N*,*N*′-bis(4-aminobiphenyl)-(1,1′-biphenyl)-4,4′-diamine pyromellitimide] (PMDA-DBABBD PI), was obtained by thermal imidization from its poly(amic acid) (PAA) made by the reaction of pyromellitic dianhydride with the DBABBD that was chemically reduced from *N*,*N*′-diphenyl-*N*,*N*′-bis(4-nitrobiphenyl)-(1,1′-biphenyl)-4,4′-diamine synthesized through the palladium-catalyzed amination. The materials were characterized by using ^{1}H NMR, ^{13}C NMR, FT-IR, HR GC-MS, EA, and DSC. The characteristics of the PAA or PI thin films were investigated with XPS and an impedance spectroscopy. The hybrid light-emitting devices (HOLEDs) with the PAA and PI thin films were fabricated to examine the performance of the polymeric thin films as a hole injecting and transporting layer. The PI thin film having the glass transition temperature of 200 °C showed stable characteristics in the application for the HOLED whereas the PAA thin film seemed to be unstable. The power efficiency of the HOLED with the PI thin film was 0.23 cd/A at 4000 cd/m^2.

Introduction

Much attention has been paid to an organic light-emitting device (OLED), an organic electroluminescent device (OELD) in more detail, because it is considered as the most prospective candidate for a flat panel display since a hole transporting organic small molecule classified as an aromatic tertiary amine derivative has been successfully applied for decreasing the working voltage of the OLED below 10 V despite its much lower hole drift mobility of approximately $10^{-3} \sim 10^{-7}$ cm^2/(V s) than the well-known inorganic semiconductor.[1,2] Because of the breakthrough of the materials and processes, the passive matrix displays using these organic small molecules have been commercialized.[3] However, a small molecule has a potential weak point such as low impact strength, interdiffusion between organic layers, and process limitation in a vacuum only. This regard motivated to develop several types of hole transporting polymers such as side-chain polymers,[4−12] main-chain polymers,[13−19] cross-linked polymers,[20−25] and polysilanes[26−29] because a polymer has generally high toughness compared to a small molecule as well as it can be processed under a wet condition which is relatively cheaper than a dry process in a vacuum. The application of these polymers for the OLED created a new category of a hybrid OLED (HOLED), which is named to differentiate it from the conventional OLED with the small molecules only.

An aromatic polyimide has been regarded as one of the high-performance polymers for a thin-film application in microelectronic devices and liquid crystal displays due to its outstanding mechanical, chemical, thermal, and physical characteristics.[30−32] In particular, the excellent planarizability of an aromatic polyimide is another reason why it can be applied as an active organic layer passing charge carriers, i.e., electrons or holes, because an uniform emission cannot be achieved if the thickness of the active layer is not same over the entire area owing to the poor planarization of organic layers. In this sense, several applications have been reported for the HOLED using the polyimides such as insoluble light-emitting polyimides,[33−37] soluble light-emitting polyimide,[38,39] insoluble hole transporting polyimides,[40−44] insoluble light-emitting molecularly doped polyimides,[45−47] soluble hole transporting molecularly doped polyimide,[48−51] and insoluble hole transporting molecularly doped polyimides.[52−56] However, an aromatic polyimide cannot practically exhibit a high luminance and efficiency owing to the quenching effect of an imide group that easily makes charge-transfer complexes.[30] Therefore, it is reasonable for a practical use as a device or display product that the actual application of the polyimide is limited to a hole injecting or transporting layer, not an emission layer (EML).

Recently, we have reported that poly[*N*,*N*′-diphenyl-*N*,*N*′-bis(4-aminobiphenyl)-(1,1′-biphenyl)-4,4′-diamine pyromellitimide] (PMDA-DBABBD PI) prepared via a vapor deposition polymerization shows an excellent thermal stability compared to the hole injecting or transporting small molecules from the examination by the capacitance−temperature measurement technique.[43] In this study, we report the synthesis and characteristics of the PMDA-DBABBD PI as well as the application for the HOLED.

* Corresponding author: e-mail ykimdaum@hanmail.net.

10.1021/ma020688v CCC: $22.00
Published on Web 10/12/2002

Experimental Section

Materials. All materials for a monomer synthesis were used as received in a reagent grade from Aldrich Chemical Co. However, further purification procedures were carried out for a poly(amic acid) synthesis because of the moisture-sensitive characteristics of a dianhydride moiety. Pyromellitic dianhydride (PMDA, **2a**) was purified by a vacuum sublimation method under the base pressure of 10^{-3} Torr. *N*-Methyl-2-pyrrolidinone (NMP) was distilled from phosphorus pentoxide to remove remnant water molecules. Tris(8-hydroxyquinolinato)aluminum (Alq3, not sublimed, TCI) and lithium−aluminum (Li:Al, 0.1% Li, RPVD Co.) alloy were used as received for the HOLED fabrication.

Synthesis of 4-Bromo-4′-nitrobiphenyl (1b). 4-Bromobiphenyl (4.66 g, **1a**, Aldrich) was added to a mixture containing sulfuric acid (6 g, Aldrich) and acetic acid (35 g, Aldrich) in a three-necked flask equipped with a condenser and a magnetic stirrer. After well-mixing of the mixture, 60% nitric acid (2.21 g, Aldrich) was dropped slowly thereto at 25 °C for 5 min, followed by continuous heating of the mixture at 75 °C for 4 h. Then the reaction mixture was cooled to room temperature, and the precipitates were filtered with a glass filter. The filtrates were washed with deionized water and dried at 60 °C for 3 days. The dried product, 4-bromo-4′-nitrobiphenyl (**1b**), was a white solid, and the final weight was 4.4 g (yield 80%); mp 177.2 °C. MS *m*/*e* Calcd: 276.99 (M^+). Found: 277.06 (M^+). ^{1}H NMR ($CDCl_3$): δ 8.24 (d, 2H-3′,5′, B), 7.68 (d, 2H-2′,6′, B), 7.57 (d, 2H-3,5, A), 7.44 (d, 2H-2,6, A). ^{13}C NMR ($CDCl_3$): δ 146.3 (1C-4′, B), 142.7 (1C-1′, B), 137.6 (1C-1, A), 132.3 (2C-3,5, A), 128.9 (2C-2,6, A), 127.6 (2C-2′,6′, B), 124.2 (2C-3′,5′, B), 123.5 (1C-4, A). Elemental Anal. Calcd for $C_{12}H_8Br_1N_1O_2$: C, 51.83; H, 2.90; Br, 28.73; N, 5.04; O, 11.51. Found: C, 51.73; H, 2.89; Br, not measured; N, 5.10; O, not measured.

Synthesis of *N*,*N*′-Diphenyl-*N*,*N*′-bis(4-nitrobiphenyl)-(1,1′-biphenyl)-4,4′-diamine (1d). 4-Bromo-4′-nitrobiphenyl (2.92 g, **1b**), *N*,*N*′-diphenylbenzidine (1.68 g, **1c**), palladium(II) acetate (55 mg, Aldrich), and tri-*o*-tolylphosphine (220 mg, Aldrich) were added to a refined xylene (10 mL, Aldrich) and stirred until a well-mixed solution. Sodium *tert*-butoxide (1.25 g, Aldrich) was added thereto under a nitrogen atmosphere. Then the mixture was heated at 120 °C for 3 h. After finishing the reaction, the reacted mixture was cooled to room temperature, and chloroform (50 mL, Aldrich) was added thereto. The resulting solution was filtered, and the solvent was removed from the filtrate under a reduced pressure. The residue was purified by a silica gel column chromatography with the mixture of chloroform and *n*-hexane (50:50) as an eluent. The purified product, *N*,*N*′-diphenyl-*N*,*N*′-bis(4-nitrobiphenyl)-(1,1′-biphenyl)-4,4′-diamine (DBNBBD, **1d**), was 2.63 g (yield 72%); mp: not detected. MS *m*/*e* Calcd: 730.26 (M^+). Found: 730.25 (M^+). ^{1}H NMR (DMSO-d_6): δ 8.27−8.24 (d, 4H-2,6, A), 7.93−7.89 (d, 4H-3,5, A), 7.75−7.72 (d, 8H-3,5, B, C), 7.63−7.60 (d, 4H-3,5, D), 7.40−7.35 (t, 8H-2,6, B, C), 7.17−7.07 (m, 6H, D). ^{13}C NMR (DMSO-d_6): δ 146.0 (2C-1, A), 130.9 (4C-1, B, C), 129.8 (4C-4, B, C), 128.4 (4C-3,5, D), 127.5 (8C-3,5, B, C), 126.9 (4C-3,5, A), 125.1 (2C-4, D), 124.6 (8C-2,6, B, C), 124.1 (4C-2,6, D), 122.5 (4C-2,6, A). Elemental Anal. Calcd for $C_{48}H_{34}N_4O_4$: C, 78.89; H, 4.49; N, 7.67; O, 8.76. Found: C, 78.90; H, 4.93; N, 7.59; O, 8.58.

Synthesis of *N*,*N*′-Diphenyl-*N*,*N*′-bis(4-aminobiphenyl)-(1,1′-biphenyl)-4,4′-diamine (1e). The DBNBBD (1.46 g, **1d**) and sodium hydrosulfide (0.64 g, 70% solution, Aldrich) were added to a three-necked flask filled with a mixture of *n*-butyl alcohol (25 mL, Aldrich) and deionized water (2 mL). Then the mixture was heated at 110 °C for 24 h for the chemical reduction reaction. After cooling the reaction mixture to room temperature, the solvent was distilled off under a reduced pressure. The resulting residue was washed with deionized water (10 mL) for several times and filtered with a glass filter. Finally, the filtrates were dried in a vacuum oven at 75 °C for 4 days. The weight of the product, *N*,*N*′-diphenyl-*N*,*N*′-bis(4-aminobiphenyl)-(1,1′-biphenyl)-4,4′-diamine (DBABBD, **1e**), was 1.16 g (yield 91%); mp: not detected. MS *m*/*e* Calcd: 670.31 (M^+). Found: 670.31 (M^+). ^{1}H NMR (DMSO-d_6): δ 7.58−7.48 (d, 12H-3,5, A, B), 7.35−7.30 (d, 4H-3,5, D), 7.09−7.03 (d, 2H-4, D), 6.64 (d, 12H-2,6, A, B, C), 6.61 (d, 4H-2,6, D), 5.21 (d, 4H, amino). ^{13}C NMR (DMSO-d_6): δ 148.1 (2C-1, A), 147.1 (2C-4, A), 146.2 (4C-1, B), 135.8 (4C-4, B), 129.5 (4C-3,5, A), 127.1 (8C-3,5, B), 126.8 (4C-3,5, A), 123.8 (2C-4, D), 123.3 (4C-2,6, D), 122.9 (8C-2,6, B, C), 114.3 (4C-2,6, A). Elemental Anal. Calcd for $C_{48}H_{38}N_4$: C, 85.94; H, 5.71; N, 8.35. Found: C, 86.63; H, 5.85; N, 8.29.

Synthesis of Poly[*N*,*N*′-diphenyl-*N*,*N*′-bis(4-aminobiphenyl)-(1,1′-biphenyl)-4,4′-diamine pyromellitamic acid] (2c). PMDA (1.09 g, Aldrich, **2a**) was slowly added to a solution of the DBABBD (3.35 g, **1e**) in NMP (82.06 mL) in a glovebox charged with a dried argon gas. The solution was further stirred for the polymerization reaction at room temperature for 48 h. Then the solution was poured into methanol (1500 mL) with vigorous stirring. The precipitate was filtered with a glass filter. For several times, the filtrate was dissolved in NMP and subsequently precipitated into methanol in order to remove some parts of impurities and low molecular weight residues. The finally purified filtrate was dried at 60 °C for 12 h in a vacuum oven. The dried product, poly[*N*,*N*′-diphenyl-*N*,*N*′-bis(4-aminobiphenyl)-(1,1′-biphenyl)-4,4′-diamine pyromellitamic acid] (PMDA-DBABBD PAA) (**2b**), was 3.2 g (yield 72.1%). FT-IR (KBr pellet): 3295 (amide N−H stretching), 3030 (aromatic Ar−H), 3400−2400 (carboxylic acid O−H), 1730 (carboxylic acid C═O), 1660 (amide C═O), 1592 (amide N−H bending), 1316−1277 (amide C−N), 825 (amide N−H out-of-plane bending), 900−500 cm^{-1} (aromatic C−H out-of-plane bending).

Thin-Film Fabrication. To measure the optical absorption and the photoluminescence (PL), the DBABBD thin film was deposited onto a quartz substrate by a resistive thermal evaporation process in a vacuum of 10^{-7} Torr. The thickness of the DBABBD thin film was 500 Å. The 2 wt % solution of the PAA in NMP was spin-coated onto a quartz substrate and an indium−tin oxide (ITO) glass for the measurement of the optical absorption and the surface composition, respectively. The PAA thin film was soft-baked at 80 °C for 4 h and followed by thermal imidization at 250 °C for 2 h, leading to the PI thin film. The thickness of the PAA and PI thin films was 240 and 150 Å, respectively.

Device Fabrication. Two kinds of devices were fabricated: one is a hole-only device (HOD) and another a HOLED. The ITO glass was patterned in a strip size of 2 mm × 30 mm. The patterned ITO glass was ultrasonically cleaned in deionized water with a non-phosphorus detergent and finally washed in ethanol before drying. To make the HOD, the same procedures as used in the PI thin-film fabrication were applied, except for the different spinning speed. Next the aluminum was deposited on top of the PI thin film by the thermal evaporation in a vacuum chamber. The thickness of the PI thin film and the aluminum electrode was 500 and 2500 Å, respectively. For the fabrication of the HOLED, the same PAA and PI thin films as prepared in the thin film fabrication were coated as a hole injecting and transporting layer (HITL) onto the patterned ITO glass. On top of the PAA and PI thin films, the 600 Å thick Alq3 thin film as an EML was deposited and followed by the evaporation of the Li:Al cathode. As a final step, the HOLEDs were encapsulated with a stainless can and a calcium oxide type desiccant.

Measurements. ^{1}H NMR and ^{13}C NMR spectra were acquired by using a Fourier transform nuclear magnetic resonance system (FT-NMR, Varian Unity Plus 300, 300 MHz, Varian). An element analysis was conducted with an elemental analyzer (EA, Vario EL, Elemental Analysen Systeme). The molecular mass of the synthesized materials was measured by using a high-resolution gas chromatography−mass (HR GC-MS) system (Profile HV-3, KRATOS). The infrared transmission spectrum of the powders was obtained with a Fourier transform infrared spectrometer (FT-IR, Protégé 460, Nicolet). An ultraviolet−visible spectrophotometer (UV−vis, Perkin-Elmer Lambda 9) was used for the measurement of the optical absorption spectra of the thin films. A melting point and a glass transition temperature were measured with a differential

Scheme 1. Synthetic Routes for 4-Bromo-4′-nitrobiphenyl, BDNBBD, and DBABBD

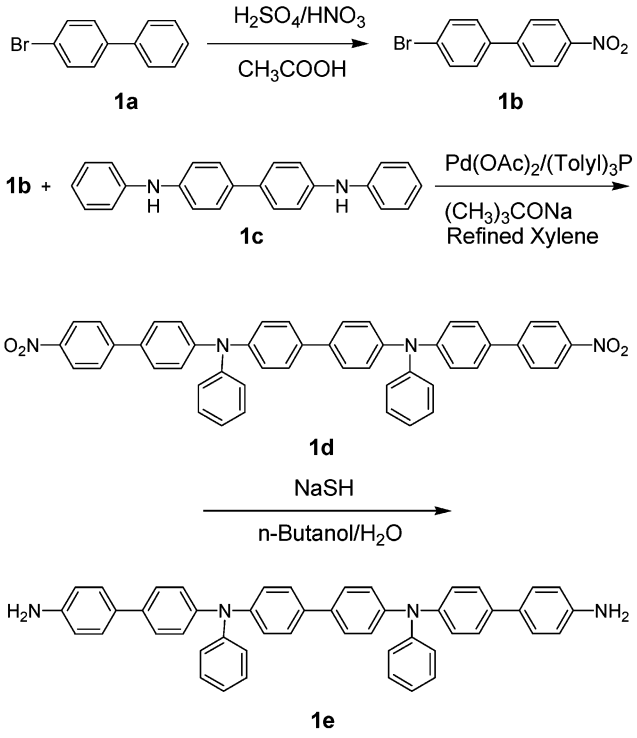

scanning calorimeter (DSC 2910, TA Instruments Inc.) as a typical ramp rate of 10 °C/min. The surface composition of the PAA and PI thin films was analyzed by using an X-ray photoelectron spectroscopy multitechnique system (XPS, PHI 5700) equipped with a monochromatic Al Kα X-ray source ($h\nu$ = 1486.6 eV). A photoluminescent (PL) spectrum was measured with a spectroscopy system (JOBIN-YVON 270M, SPEX Instruments Inc.) equipped with a monochromator and a photomultiplier tube. The capacitance of the thin films was measured with an impedance analyzer (4192A, Hewlet-Packard). The luminance−voltage and electroluminescent (EL) characteristics were obtained with an electrical measurement system equipped with an electrometer (SMU237, Keithley) and a candela meter (PR650, Photo Research Inc.). The thickness of all thin films was measured by using a surface profiler (P-10, Tencor).

Results and Discussion

Synthesis of Monomers and Polymer. 4-Bromo-4′-nitrobiphenyl (**1b**) was easily obtained with the average yield of 80% as shown in Scheme 1 by the direct nitration of 4-bromobiphenyl (**1a**) in the presence of the mixed acid solution of concentrated sulfuric acid, nitric acid, and acetic acid.[57] The results are shown in Figure 1. The found mass was almost similar to the calculated one. The ^{1}H NMR and ^{13}C NMR spectra show clearly the peak split owing to the different environment of protons and carbons after the nitration reaction.

The DBNBBD (**1d**) was synthesized with the palladium-catalyzed amination reaction reported by Yamamoto et al.[58] It was observed through a thin-layer chromatography tracing technique that a monosubstituted compound was dominant at the initial stage, but it gradually disappeared with time whereas the population of a disubstituted derivative became rich. The characterization results are shown in Figure 2. The found mass almost exactly coincided with the calculated one. No proton peaks in the chemical shift below 7 ppm where the secondary amine protons generally appear

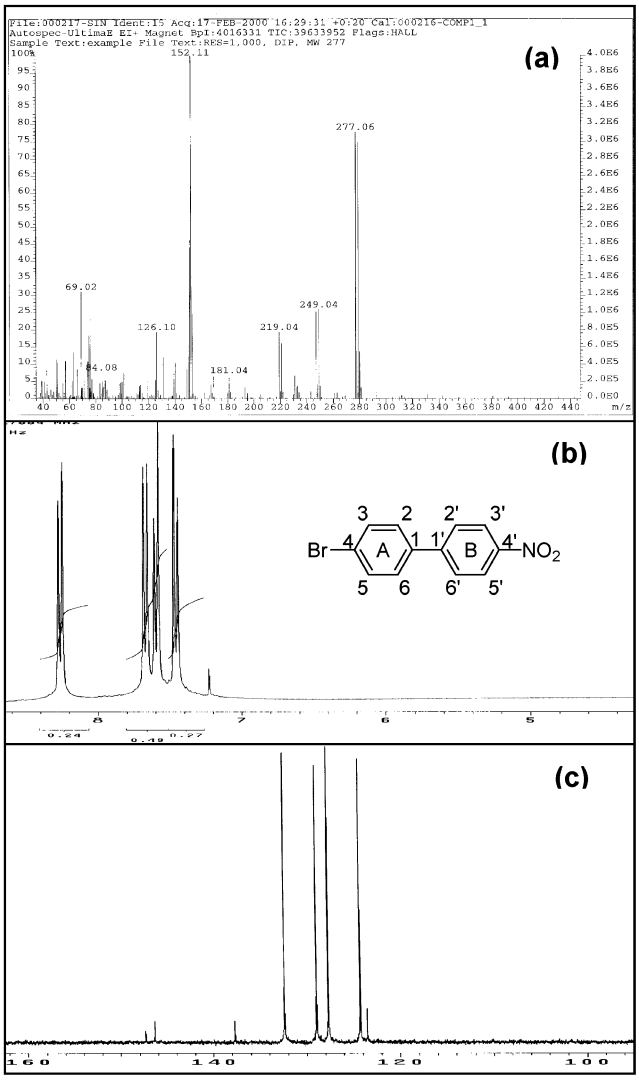

Figure 1. HR GC-MS (a), ^{1}H NMR (b), and ^{13}C NMR (c) spectra of 4-bromo-4′-nitrobiphenyl synthesized in this work.

prove that the tertiary amine was successfully made by the present amination reaction.

The DBNBBD (**1d**) was converted into the DBABBD (**1e**) by the reduction reaction utilizing sodium hydrosulfide as a catalyst. As shown in Figure 3, the found mass shows the same value as calculated. Both the proton peak at around 5.51 ppm and the carbon peak below 120 ppm reveal the formation of amino groups reduced from the nitro groups in the DBNBBD molecule.

Scheme 2 shows the schematic drawing for the polymerization of the PAA (**2b**) from the DBABBD (**1e**) and PMDA (**2a**). The polymerization reaction was performed at room temperature, but at the initial stage of the reaction some heat was monitored corresponding to the exothermic reaction frequently occurred in the conventional polymerization of a poly(amic acid). When the reaction time was 48 h, there was no more increase in the viscosity of the reaction medium. So at this time the reaction was terminated, and the solution was worked up to the solid state. Figure 4 shows the FT-IR spectrum of the PAA (**2b**) powder. From the characteristic transmission peaks such as 3295 cm^{-1} for an amide N−H stretching, 1660 cm^{-1} for an amide C═O stretching, 1592 cm^{-1} for an amide N−H bending, 1316−1277 cm^{-1} for an amide C−N bending, and 825 cm^{-1} for an

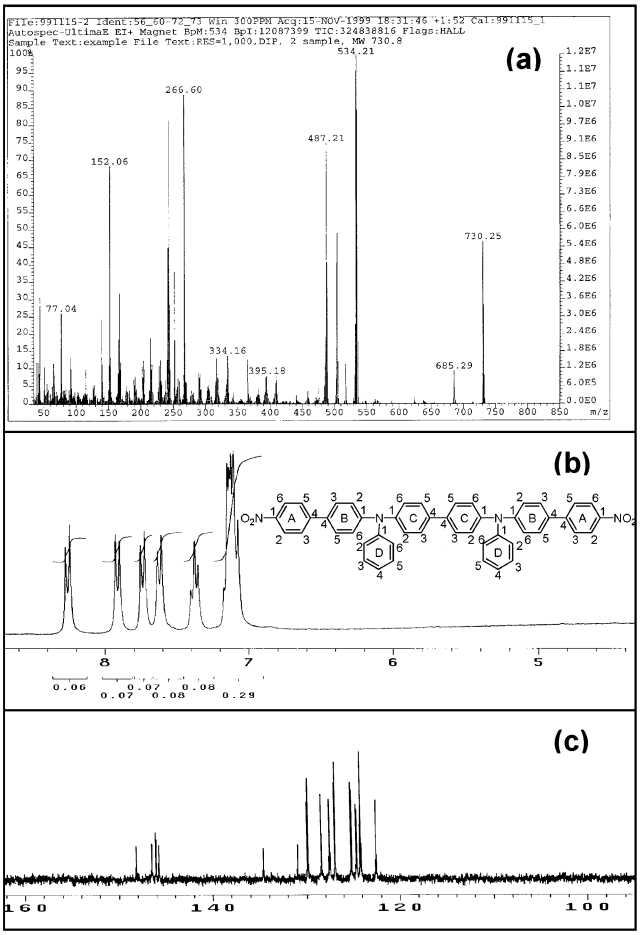

Figure 2. HR GC-MS (a), ^{1}H NMR (b), and ^{13}C NMR (c) spectra of DBNBBD synthesized in this work.

amide N−H out-of-plane bending, it was disclosed that the amide group was actually created by the reaction between the amines in the DBABBD (**1e**) and the dianhydrides in PMDA (**2a**). The color of the poly(amic acid) was slightly yellowish.

Thermal Property of Monomer and Polymer. Figure 5 shows the DSC thermogram of the DBABBD powder obtained from the third run after the first heating and second quenching runs in order to remove a previous thermal history induced during the synthesis procedures. The glass transition started at ca. 125 °C, and the glassy phase changed into an amorphous state at ca. 135 °C. No melting was detected by the DSC experiment even above 330 °C. In Figure 6A, the thermal imidization condition of the PAA powder was examined by raising the temperature up to 250 °C and keeping it isothermal for ca. 130 min. The thermal dehydration reaction initialized at around 100 °C, and the most significant change was taken place at ca. 145 °C. The change was continued up to 250 °C. From the level-off time of the heat flow in the inset figure, the time for the complete thermal imidization is assumed to be approximately 70 min. This sample was cooled to room temperature and run again to measure the glass transition temperature as shown in Figure 6B. The glass transition started at ca. 230 °C and finished at ca. 290 °C. This transition over a long temperature range is very similar to a typical transition behavior of a polymer rather than a small molecule (monomer).

Optical Properties of Monomeric and Polymeric Thin Films. The UV−vis absorption and PL spectra of

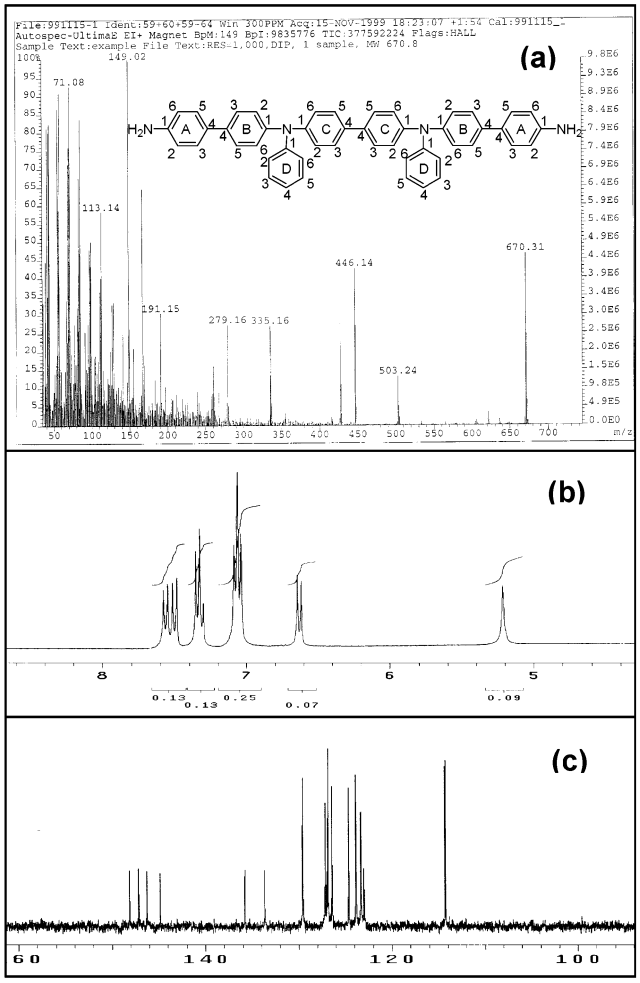

Figure 3. HR GC-MS (a), ^{1}H NMR (b), and ^{13}C NMR (c) spectra of DBABBD synthesized in this work.

Scheme 2. Synthetic Routes for PMDA-DBABBD PAA and PMDA-DBABBD PI

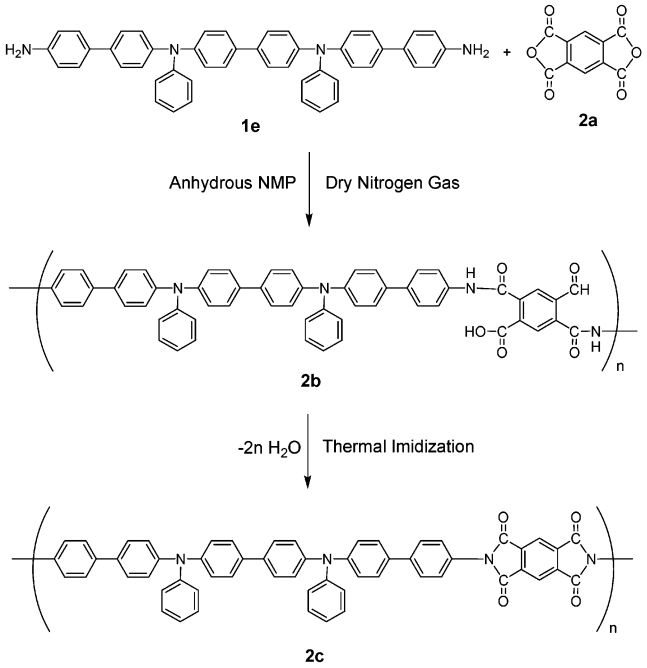

the DBABBD (**1e**) thin film on a quartz substrate are shown in Figure 7. The optical band gap of the thin film can be calculated as approximately 2.95 eV from the

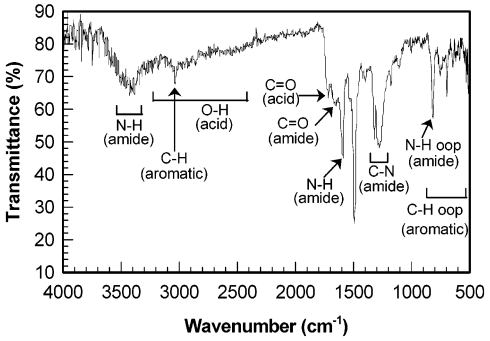

Figure 4. FT-IR spectrum of the PMDA-DBABBD PAA powder.

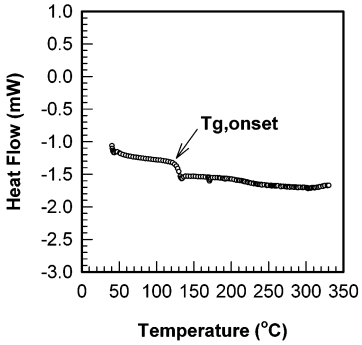

Figure 5. DSC thermogram of the DBABBD powder.

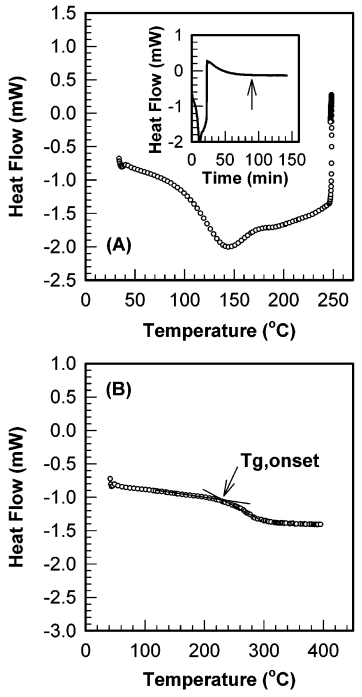

Figure 6. DSC thermogram of the PMDA-DBABBD PAA (A) and PMDA-DBABBD PI (B) powders.

onset wavelength of ca. 420 nm in the absorption spectrum. The wavelength exhibiting a maximum PL intensity was ca. 440 nm with a medium-intensity shoulder at ca. 480 nm. It is regarded from the optical absorption properties that the DBABBD (**1e**) thin film itself can be used as a blue EML as well as a HTL even though the accurate band energy levels such as an ionization potential and an electron affinity should be measured. Figure 8 shows the absorption spectrum of the PAA and PI thin films coated onto a quartz

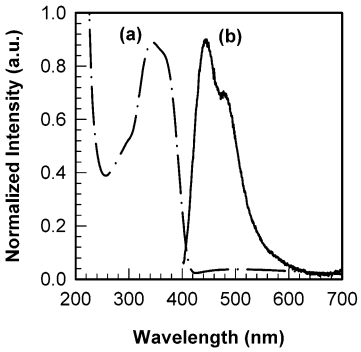

Figure 7. Optical absorption (a) and photoluminescence (b) spectra of the DBABBD thin film on a quartz substrate.

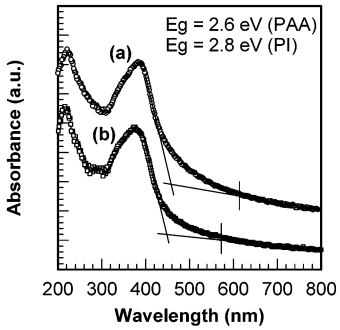

Figure 8. Optical absorption spectra of the PMDA-DBABBD PAA (a) and PMDA-DBABBD PI (a) thin films on a quartz substrate.

substrate. The shape of the absorption spectra resembles that of the DBABBD thin film with a marginal spectral shift toward a low-energy region. The baselines shown in the figure were drawn in order to calculate the optical band gap because the onset point is not clearly observed for both the PAA and PI thin films. On the basis of the baselines, the optical band gaps were calculated as approximately 2.6 and 2.8 eV for the PAA and PI thin films, respectively. However, it should be noted from the weak absorption at the longer wavelength above 450 nm that there is a possible formation of other gap states. For both the PAA and PI thin films, the PL was almost undetectable at the excitation of 365 nm. This is why the electrons in the excited state pumped optically from the ground state or the excitons generated are trapped and then disappeared by a nonradiative energy transfer process owing to the intramolecular or intermolecular charge transfer (CT) complex formed between the carbonyl group as an acceptor and the aromatic or amino group as a donor even though a fluorescent emission has been reported for some polyimide systems.[30] In this regard, it can be assumed that the weak absorption at the longer wavelength region is originated from the CT complexes in the polymeric thin films.

Surface Characteristics of the PAA and PI Thin Films. Figure 9 shows the deconvoluted C 1s core level XPS spectrum for the surface of the PAA and PI thin films. The PAA thin film surface has several characteristic C 1s peaks at 284. eV for aromatic C−C bonds, 284.8 eV for C−N bonds, 285.8 eV for carboxylic acid C−O bonds, 287.9 eV for amide C═O bonds, and 288.8 eV for carboxylic acid C═O bonds. It is proved again that the PAA was really synthesized because its film surface has two different carbonyl C 1s peaks, meaning the different electronic environments. However, the PI thin film shows the single C 1s carbonyl peak at 288.7

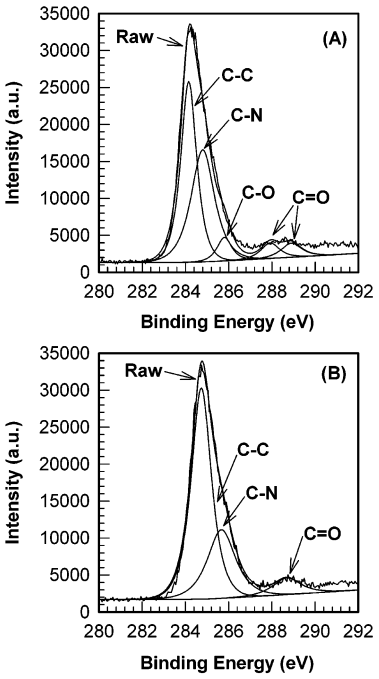

Figure 9. XPS spectra of the PMDA-DBABBD PAA (A) and PMDA-DBABBD PI (B) thin films on an ITO glass substrate.

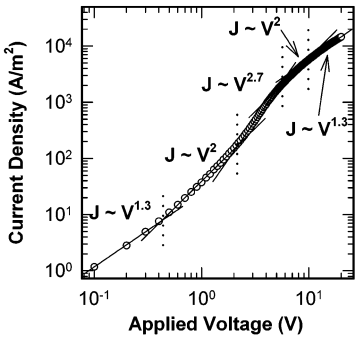

Figure 10. Variation of the current density as a function of applied voltage for the HOD consisted of glass/ITO/PMDA-DBABBD PI/Al.

eV, meaning that the carbon atom in the carbonyl group exists under the same electronic environment. This is why only imide groups were made by the dehydration reaction between the carboxylic acid and amide groups of the poly(amic acid) during the thermal imidization process. In addition, no C−O peak for a carboxylic acid is another evidence for the successful imidization. In particular, more increased binding energy is observed for the C−C (284.7 eV) and C−N (285.6 eV) bonds in the PI thin-film surface than the PAA thin film. It is considered that this binding energy increase is owing to the increased packing density between the PI chains during the thermal imidization process.

Characteristics of HODs. The current density−voltage ($J-V$) characteristic of the HOD fabricated with the PI thin film is shown in Figure 10. The $J-V$ plot shows the typical regimes such as an ohmic ($m = 0.3$), a space charge limited ($m = 1$), a trap charge limited ($m = 1.7$), and a trap-free space charge limited ($m = 1$) in the power-law model ($J \approx V^{m+1}$).[51] In addition to the typical regimes, another regime ($m = 0.3$) similar to an ohmic was observed at high electric field. From the relatively low m value compared to the other reports,[51] it is considered that a small trap state exists in the present HOD even though the device passes hole carriers only. The ionization potential of the PI thin film on the ITO substrate was obtained as 5.12 eV by the ultraviolet photoelectron spectroscopy (UPS) method described in the previous work.[59] The difference in the UPS measurement is that the present work applied the spin-coating as the preparation method of the thin film while a thermal evaporation was used in the previous work. As shown in Figure 11, the energy band diagram of the HOD can be built on the basis of the ionization potential and the work function of the ITO.[60] From this energy band diagram, it is clear that the present HOD mainly passes a hole rather than an electron because of the higher barrier between the conduction band of the PI thin film and the Al electrode.

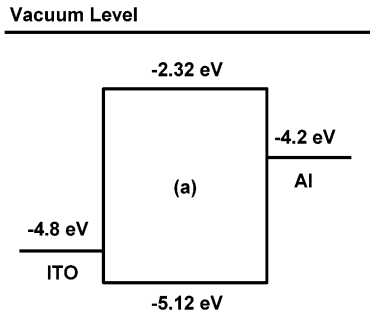

Figure 11. Energy band diagram of the HOD consisted of glass/ITO/PMDA-DBABBD PI/Al.

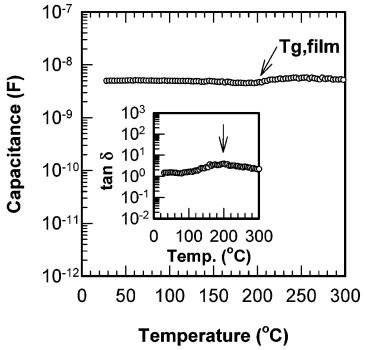

Figure 12. Variation of the capacitance and the dissipation factor (inset) as a function of temperature for the HOD consisted of glass/ITO/PMDA-DBABBD PI/Al at 1 kHz.

Figure 12 shows the variation of the capacitance as a function of temperature at the frequency of 1 kHz. The capacitance was almost not changed below 200 °C, meaning no further reactions by the other causes, except the space charges, affecting the capacitance increase described in Figure 12A. However, the capacitance was changed at around 200 °C and slightly became higher. This is owing to the increased electrical resistance in the film as well as the distorted or degraded interface between the PI thin film and the electrodes by the PI main-chain relaxation at around the glass transition temperature. The relaxation behavior was also observed from the dissipation factor in the inset figure. The capacitance−temperature ($C-T$) result indicates that the glass transition temperature of the PI thin film is about 200 °C. Here it is noteworthy that the glass transition temperature of the PI thin film is almost 30 °C lower than that of the PI powder as shown in Figure 6.

Characteristics of HOLEDs. Figure 13 shows the characteristics of the HOLED with the PAA thin film as a HITL. The turn-on voltage is ca. 8 V while the first charge injection occurs at ca. 3 V in the presence of a

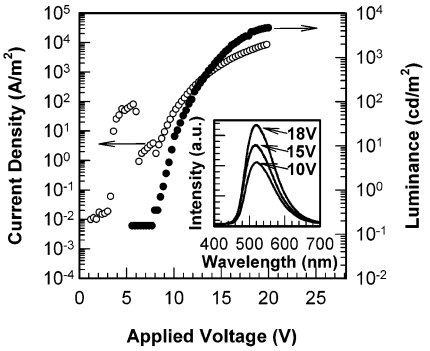

Figure 13. Variation of the current density and the luminance as a function of applied voltage for the HOLED consisted of glass/ITO/PMDA-DBABBD PAA/Alq3/Li:Al. The inset figure shows the EL spectra with the applied voltage.

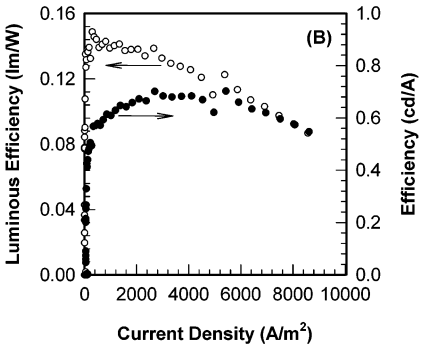

Figure 14. Variation of the device efficiency as a function of current density for the HOLED consisted of glass/ITO/PMDA-DBABBD PAA/Alq3/Li:Al.

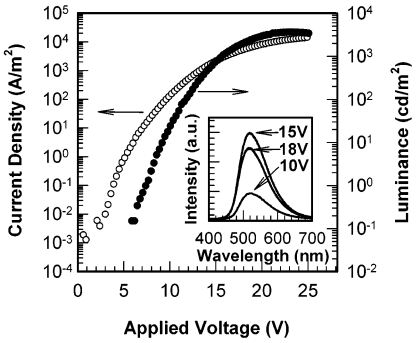

Figure 15. Variation of the current density and the luminance as a function of applied voltage for the HOLED consisted of glass/ITO/PMDA-DBABBD PI/Alq3/Li:Al. The inset figure shows the EL spectra with the applied voltage.

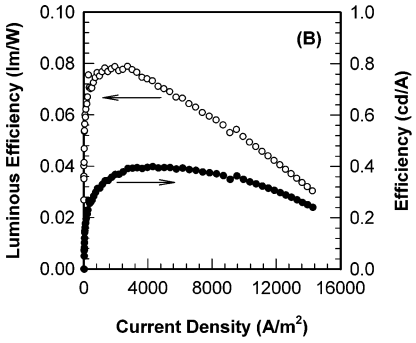

Figure 16. Variation of the device efficiency as a function of applied voltage and the current density for the HOLED consisted of glass/ITO/PMDA-DBABBD PI/Alq3/Li:Al.

current bump at around 3−5 V. Therefore, the balanced injection of the electrons and holes is not achieved for the present device. It is thought that the major cause for the unbalance is mainly ascribed to the charge accumulation near the PAA-Alq3 interface even though the space charge effect still exists at the PI thin film−electrode interface. To emit a light, the hole carriers have to transport into the Alq3 emission zone, but most of them are blockaded at the interface owing to the relatively large difference in the ionization potential between the PAA and Alq3 layers. However, the accurate investigation should be further carried out with the whole energy band diagram. Unfortunately, it is not available at present because the ionization potential of the PAA thin film could not be obtained with the UPS method owing to the unstable signal of the photoelectrons from the PAA thin film in an ultrahigh-vacuum (UHV) chamber.[59] The major cause of the unstable signal is the inherently unstable characteristic of the PAA material, which is generally called as a precursor meaning an intermediate. In addition, the remnant solvent molecules captured between the PAA chains are also one of the causes for the unstable UPS signal because it can play as an outgas under an UHV condition. The current bump at the low voltage may be one of the proofs for the unstable status of the PAA thin film even though one can regard it as a typical pinhole-like defect. Despite these problems, the maximum luminance reached ca. 5000 cd/m^2 at 20 V. The EL spectrum was not changed with the applied voltage as shown in the inset figure. Figure 14 shows the efficiency behavior of the HOLED with the PAA thin film as a function of current density. The power efficiency shows a parabolic behavior with the current density whereas the luminous efficiency decreases monotonically exhibiting a maximum at very low current density. The maximum power efficiency was ca. 0.7 cd/A.

Unlike the HOLED with the PAA thin film, no current bump is observed from the $J-V$ plot of the HOLED with the PI thin film in Figure 15. This is considered as a result of the stable characteristic of the PI thin film as well as the repaired pinholes, if any, during the thermal imidization process. However, the HOLED with the PI thin film is also regarded as an unbalanced device because the voltage difference between the charge injection (ca. 2 V) and the turn-on (ca. 6 V) is still large. The maximum luminance of ca. 4000 cd/m^2 was achieved in the presence of the saturated light emission above 20 V. The EL spectra having the peak at ca. 520 nm were not significantly shifted with the applied voltage as shown in the inset figure. The efficiency behavior is somewhat similar to the HOLED with the PAA thin film as shown in Figure 16. However, the HOLED with the PI thin film exhibited almost a half value in the power efficiency compared to that with the PAA thin film. This means that the present device with the PI thin film is relatively less balanced than that with the PAA thin film. The unbalanced injection can be expected from the band diagram shown in Figure 17.[61] The electron injection from the Li:Al cathode into the conduction band of the Alq3 layer is easier than the hole transport from the valence band of the PI thin film into that of the Alq3 layer. That is, most of the hole carriers reside at the valence band of the PI thin film owing to the large energy barrier height of ca. 0.78 eV while the electrons exist at the conduction band of the Alq3 layer. This confinement of both carriers acts as a space charge leading to the reduction in the internal voltage across both electrodes. Consequently, it results

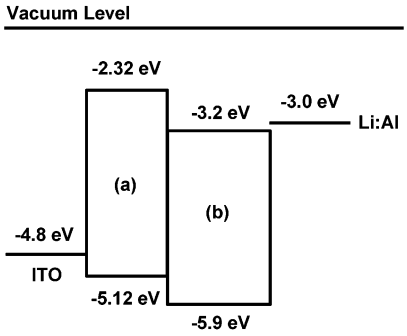

Figure 17. Energy band diagram of the HOLED consisted of glass/ITO/PMDA-DBABBD PI/Alq3/Li:Al.

in the degradation of the device performance. From the viewpoint of this barrier height explanation affecting the device performance, it is considered that the ionization potential of the PAA thin film may be higher than that of the PI thin film because the HOLED with the PAA thin film shows higher efficiency than that with the PI thin film. To overcome the unbalanced recombination between electrons and holes, a HTL having a suitable ionization potential of desirably 5.4 eV should be introduced between the PI thin film and the Alq3 layer.[61] In addition, the application of an insulating electron injecting layer such as LiF is also helpful to adjust the electron injection against the minor holes diffused from the anode side.[62]

Conclusions

The hole injecting and transporting polyimide, PMDA-DBABBD PI, was prepared from its soluble precursor, PMDA-DBABBD PAA, which was synthesized with PMDA and the DBABBD obtained from DBNBBD. The onset temperature of the glass transition for the DBABBD and PI powders was 125 and 230 °C, respectively. However, the glass transition temperature of the PI thin film decreased to 200 °C. The band gap energy of the PAA thin film was 2.6 eV while that of the PI thin film was 2.8 eV, which are slightly narrower than that of the DBABBD thin film. The C 1s peak related to the carbonyl group of the PI thin film was single whereas two C 1s peaks were observed for the PAA thin film. It means that the PAA was successfully converted into the PI by thermal imidization. The HOLED with the PAA thin film was unstable in the current injection because of the inherent imperfectness of the PAA itself. Although both HOLEDs with the PAA and PI thin films exhibited a high luminance more than 4000 cd/m^2, they seem to be unbalanced with regard to the low efficiency as well as the big difference between the charge carrier injection and the turn-on of light. In conclusion, it is expected that the HOLED with the PI thin film should have excellent performance once the ionization potential of the PI thin film is modified or other guest HTL is included between the PI thin film and the anode.

Acknowledgment. The authors thank Y. Y. Jeong, D. K. Choi, S. S. Park, and H. Lim for their support in the fabrication and the measurement of the devices. The partial financial support by National Research Laboratory program is greatly acknowledged.

References and Notes

(1) Tang, C. W.; VanSlyke, S. A. *Appl. Phys. Lett.* **1987**, *51*, 913.
(2) Forrest, S. R. *IEEE J. Sel. Top. Quantum Electron.* **2000**, *6*, 1072.
(3) Mahon, J. K. *SID 01 Digest* **2001**, 22.
(4) Bouché, C.-M.; Berdagué, P.; Facoetti, H.; Robin, P.; Le Barny, P.; Schott, M. *Synth. Met.* **1996**, *81*, 191.
(5) Kolb, E. S.; Gaudiana, R. A.; Mehta, P. G. *Macromolecules* **1996**, *29*, 2359.
(6) Son, J. M.; Sakaki, Y.; Ogino, K.; Sato, H. *IEEE Trans. Electron Devices* **1997**, *44*, 1307.
(7) Hanai, N.; Sumitomo, M.; Yanagi, H. *Thin Solid Films* **1998**, *331*, 106.
(8) Bellmann, E.; Shaheen, S. E.; Thayumanavan, S.; Barlow, S.; Grubbs, R. H.; Marder, S. R.; Kippelen, B.; Peyghambarian, N. *Chem. Mater.* **1998**, *10*, 1668.
(9) Bellmann, E.; Shaheen, S. E.; Grubbs, R. H.; Marder, S. R.; Kippelen, B.; Peyghambarian, N. *Chem. Mater.* **1999**, *11*, 399.
(10) Shaheen, S. E.; Jabbour, G. E.; Kippelen, B.; Peyghambarian, N.; Anderson, J. D.; Marder, S. R.; Armstrong, N. R.; Bellmann, E.; Grubbs, R. H. *Appl. Phys. Lett.* **1999**, *74*, 3212.
(11) Jabbour, G. E.; Shaheen, S. E.; Morrell, M. M.; Anderson, J. D.; Lee, P.; Thayumanavan, S.; Barlow, S.; Bellmann, E.; Grubbs, R. H.; Kippelen, B.; Marder, S. R.; Armstrong, N. R.; Peyghambarian, N. *IEEE J. Sel. Top. Quantum Electron.* **2000**, *36*, 12.
(12) Tamada, M.; Koshikawa, H.; Suwa, T.; Yoshioka, T.; Usui, H.; Sato, H. *Polymer* **2000**, *41*, 5661.
(13) Kraft, A.; Burn, P. L.; Holmes, A. B. *Synth. Met.* **1993**, *55*−*57*, 4163.
(14) Stolka, M.; Abkowitz, M. A. *Polym. Prepr.* **1997**, *38*, 311.
(15) Yamamori, A.; Adachi, C.; Koyama, T.; Taniguchi, Y. *J. Appl. Phys.* **1999**, *86*, 4369.
(16) Gauvin, S.; Santerre, F.; Dodelet, J. P.; Ding, Y.; Hlil, A. R.; Hay, A. S.; Anderson, J.; Armstrong, N. R.; Gorjanc, T. C.; D'Iorio, M. *Thin Solid Films* **1999**, *353*, 218.
(17) Redecker, M.; Bradley, D. D. C.; Inbasekaran, M.; Wu, W. W.; Woo, E. P. *Adv. Mater.* **1999**, *11*, 241.
(18) Son, J. M.; Mori, T.; Ogino, K.; Sato, H.; Ito, Y. *Macromolecules* **1999**, *32*, 4849.
(19) Fukase, A.; Kido, J. *Proceeding of the 10th International Workshop on Inorganic and Organic Electroluminescence (EL'00)*; Kobayashi, H., Tsutsui, T., Eds.; Hamamatsu: 2000; p 293.
(20) Roitman, D. B.; Antoniadis, H.; Hueschen, M.; Moon, R.; Sheats, J. R. *IEEE J. Sel. Top. Quantum Electron.* **1998**, *4*, 58.
(21) Bacher, A.; Erdelen, C. H.; Paulus, W.; Ringsdorf, H.; Schmidt, H.-W.; Schuhmacher, P. *Macromolecules* **1999**, *32*, 4551.
(22) Bayerl, M. S.; Braig, T.; Nuyken, O.; Müller, D. C.; Gross, M.; Meerholz, K. *Macromol. Rapid Commun.* **1999**, *20*, 224.
(23) Chen, J. P.; Klaerner, G.; Lee, J. I.; Markiewicz, D.; Lee, V. Y.; Miller, R. D.; Scott, J. C. *Synth. Met.* **1999**, *107*, 129.
(24) Chen, J. P.; Markiewicz, D.; Lee, V. Y.; Klaerner, G.; Miller, R. D.; Scott, J. C. *Synth. Met.* **1999**, *107*, 203.
(25) Muller, D.; Gross, M.; Meerholz, K.; Braig, T.; Bayerl; M. S.; Bielefeldt, F.; Nuyken, O. *Synth. Met.* **2000**, *111*−*112*, 31.
(26) Kido, J.; Nagai, K.; Okamoto, Y.; Skotheim, T. *Appl. Phys. Lett.* **1991**, *59*, 2760.
(27) Hiramoto, M.; Sakata, Y.; Yokoyama, M. *Jpn. J. Appl. Phys.* **1996**, *35*, 4809.
(28) Suzuki, H.; Hoshino, S. *J. Appl. Phys.* **1996**, *79*, 858.
(29) Adachi, A.; Manhart, S. A.; Okita, K.; Kido, J.; Ohshita, J.; Kunai, A. *Synth. Met.* **1997**, *91*, 333.
(30) *Polyimides: Fundamentals and Applications*; Ghosh, M. K., Mittal, K. L., Eds.; Marcel Dekker: New York, 1996.
(31) *Recent Advances in Polyimide Science and Technology*; Weber, W. D., Gupta, M. R., Eds.; Society of Plastic Engineers: New York, 1987.
(32) *Polyimides: Materials, Chemistry and Characterization*; Feger, C., Khojasteh, M. M., McGrath, J. E., Eds.; Elsevier: Amsterdam, 1989.
(33) Tesirogi, Y. *J. Polym. Sci., Part A*: *Polym. Chem.* **1993**, *31*, 585.
(34) Wu, A.; Akagi, T.; Jikei, M.; Kakimoto, M.; Imai, Y.; Ukishima, S.; Takahashi, Y. *Thin Solid Films* **1996**, *273*, 214.
(35) Spiliopoulos, I. K.; Mikroyannidis, J. A. *Macromolecules* **1998**, *31*, 515.
(36) Pyo, S. M.; Kim, S. I.; Shin, T. J.; Ree, M.; Park, K. H.; Kang, J. S. *Polymer* **1998**, *40*, 125.

(37) Ng, W. Y.; Gong, X.; Chan, W. K. *Chem. Mater.* **1999**, *11*, 1165.
(38) Mal'tsev, E.; Berendyaev, V. I.; Brusentseva, M. A.; Tameev, A. R.; Kolesnikov, V. A.; Kozlov, A. A.; Kotov, B. V.; Vannikov, A. V. *Polym. Int.* **1997**, *42*, 404.
(39) Mal'tsev, E.; Brusentseva, M. A.; Kolesnikov, V. A.; Berendyaev, V. I.; Kotov, B. V.; Vannikov, A. V. *Appl. Phys. Lett.* **1997**, *71*, 3480.
(40) Wu, A.; Jikei, M.; Kakimoto, M.; Imai, Y.; Ukishima, S.; Takahashi, Y. *Chem. Lett.* **1994**, 2319.
(41) Wu, A.; Jikei, M.; Kakimoto, M.; Imai, Y.; Ukishima, S.; Takahashi, Y. *Mol. Cryst. Liq. Cryst.* **1995**, *267*, 441.
(42) Wu, A.; Kakimoto, M. *Adv. Mater.* **1995**, *7*, 812.
(43) Kim, Y.; Lee, J. G.; Han, K.; Hwang, H.-K.; Choi, D.-K.; Jung, Y.-Y.; Keum, J.-H.; Kim, S.; Park, S.-S.; Im, W.-B. *Thin Solid Films* **2000**, *363*, 263.
(44) Wang, Y.-F.; Chen, T.-M.; Okada, K.; Uekawa, M.; Nakaya, T.; Kitamura, M.; Inoue, H. *J. Polym. Sci., Part A: Polym. Chem.* **2000**, *38*, 2032.
(45) Kim, Y.; Cho, W. J.; Ha, C. S. *Mol. Cryst. Liq. Cryst.* **1997**, *295*, 31.
(46) Wen, W.-K.; Jou, J.-H.; Chiou, J.-F.; Chang, W.-P.; Whang, W.-T. *Appl. Phys. Lett.* **1997**, *71*, 1302.
(47) Wen, W.-K.; Jou, J.-H.; Wu, H.-S.; Cheng, C.-L. *Macromolecules* **1998**, *31*, 6515.
(48) Lim, H.; Park, H.; Cho, W. J.; Ha, C. S.; Kim, Y. *Mol. Electron. Devices* **1997**, *8*, 49.
(49) Lee, J. G.; Kim, Y.; Jang, S.-H.; Kwon, S.-N.; Jeong, K. *Appl. Phys. Lett.* **1998**, *72*, 1757.
(50) Kim, Y.; Lee, J. G.; Kim. S. *Adv. Mater.* **1999**, *11*, 1463.
(51) Kim, Y.; Keum, J.; Lee, J. G.; Lim, H.; Ha, C.-S. *Adv. Mater. Opt. Eletron.* **2000**, *10*, 173.
(52) Lim, H.; Park, H.; Lee, J. G.; Kim, Y.; Cho, W.-J.; Ha, C. S. *Proc. SPIE: Polym. Photonic Devices* **1998**, *3281*, 345.
(53) Kim, Y.; Lee, J. G.; Hwang, H.; Jang, S.-H. *Mol. Cryst. Liq. Cryst.* **1998**, *316*, 251.
(54) Lee, J. G.; Choi, D. K.; Kim, Y.; Kim, S. W.; Kim, S. C.; Lee, M. H.; Jeong, K. *J. Korean Phys. Soc.* **1999**, *35*, S604.
(55) Grell, M.; Knoll, W.; Lupo, D.; Meisel, A.; Miteva, T.; Neher, D.; Nothofer, H.-G.; Scherf, U.; Yasuda, A. *Adv. Mater.* **1999**, *11*, 671.
(56) Grell, M.; Bradley, D. D. C. *Adv. Mater.* **1999**, *11*, 895.
(57) *Vogel's Text Book of Practical Organic Chemistry*; Furniss, B. S., Hannaford, A. J., Smith, P. W. G., Tatchell, A. R., Eds.; Longman Scientific & Technical: Essex, 1989.
(58) Yamamoto, T.; Nishiyama, M.; Koie, Y. *Tetrahedron Lett.* **1998**, *39*, 2367.
(59) Kim, Y.; Im, W. B.; Hwang, H. K.; Lee, J. G.; Han, K.; Kim, S. *Proc. the 1st Int'l Display Manufacturing Conference* **2000**, *1*, 431.
(60) Giebeler, C.; Andoniadis, H.; Bradley, D. D. C.; Shirota, Y. *Appl. Phys. Lett.* **1998**, *72*, 2448.
(61) Im, W. B.; Hwang, H. K.; Lee, J. G.; Han, K.; Kim, Y. *Appl. Phys. Lett.* **2001**, *79*, 1387.
(62) Hung, L. S.; Lee, S. T. *Mater. Sci. Eng.* **2001**, *B85*, 104.

MA020688V